

OPEN

An Observed Regime Shift in the Formation of Warm Core Rings from the Gulf Stream

Avijit Gangopadhyay¹, Glen Gawarkiewicz², E. Nishchitha S. Silva¹, M. Monim³ & Jenifer Clark⁴

We present observational evidence that a significant regime change occurred around the year 2000 in the formation of Warm Core Rings (WCRs) from the Gulf Stream (GS) between 75° and 55°W. The dataset for this study is a set of synoptic oceanographic charts available over the thirty-eight-year period of 1980–2017. The upward regime change shows an increase to 33 WCRs per year during 2000–2017 from an average of 18 WCRs during 1980 to 1999. A seasonal analysis confirms May–June–July as the peak time for WCR births in agreement with earlier studies. The westernmost region (75°–70°W) is least ring-productive, while the region from 65°W to 60°W is most productive. This regime shift around 2000 is detected in WCR formation for all of the four 5-degree wide sub-regions and the whole region (75°–55°W). This might be related to a reduction of the deformation radius for ring formation, allowing unstable meanders to shed more frequent rings in recent years. A number of possible factors resulting in such a regime shift related to the possible changes in reduced gravity, instability, transport of the GS, large-scale changes in the wind system and atmospheric fluxes are outlined, which suggest new research directions. The increase in WCRs has likely had an impact on the marine ecosystem since 2000, a topic worthy for future studies.

Continental shelf waters along the mid-Atlantic and northeastern US have been rapidly changing over the last ten years. Recent observational studies indicate that extreme warming conditions are occurring more frequently in the water masses from the Middle Atlantic Bight (MAB) to the Gulf of Maine/Georges Bank (GOM/GB), along and across the Shelf break Front (SBF), in the slope waters and on the Labrador Shelf all the way into the Arctic^{1–5}. Changes have been documented in circulation and water masses, ecosystem response, fisheries abundance, fish recruitment and seasonal migration^{6,7}.

Pershing *et al.*⁵ stated that during the last decade, sea surface temperature in the GOM increased at a rate faster than 99% of the global oceans. They attributed such changes to factors such as the northward excursion of the GS and changes in the Atlantic Multi-decadal Oscillation and Pacific Decadal Oscillation. These authors also maintained that such changes might have caused the collapse of the cod fishery in New England waters^{2,8,9}.

While observational evidence for change is growing, there are competing theories on how these changes are brought about. During 2012, winter and spring shelf water temperatures were the warmest on record^{2,10}. This was attributed to decreased heat loss by the ocean during winter due to a northward shift of the atmospheric Jet Stream, and consequent warming of shelf waters¹¹.

One of the major drivers of the changes in the shelf and slope waters off the US northeast coast is thought to be the latitudinal excursions of the GS bringing warm waters into the slope sea in the form of multiple Warm Core Rings (WCR) and streamers/shingles from the GS. Determining the impact of the WCRs on the shelf-slope exchange and thus on the water masses on the shelf^{12–15} is one of the priority areas of the Ocean Observatories Initiative science plan for the Pioneer Array¹⁵ and is presently a major area of active research^{11,16,17}. Their frequent occurrence and impact on the physical, chemical and biological oceanography of the Slope Sea region have been documented in the past through field observations^{18–20}, satellite imagery^{21–24} and theoretical models^{25–28}. However, a systematic study of WCR formation and distribution is necessary to understand the impact of the rings on the underlying ecosystem and its habitats.

¹School for Marine Science and Technology, University of Massachusetts Dartmouth, MA, 02747, USA. ²Woods Hole Oceanographic Institution, Woods Hole, MA, 02543, USA. ³RPS Group, 55 Village Square Drive, South Kingstown, RI, 02879, USA. ⁴Jenifer Clark's Gulfstream, 3160 Lacrosse Court, Dunkirk, MD, 20754, USA. Correspondence and requests for materials should be addressed to A.G. (email: avijit.gangopadhyay@umassd.edu)

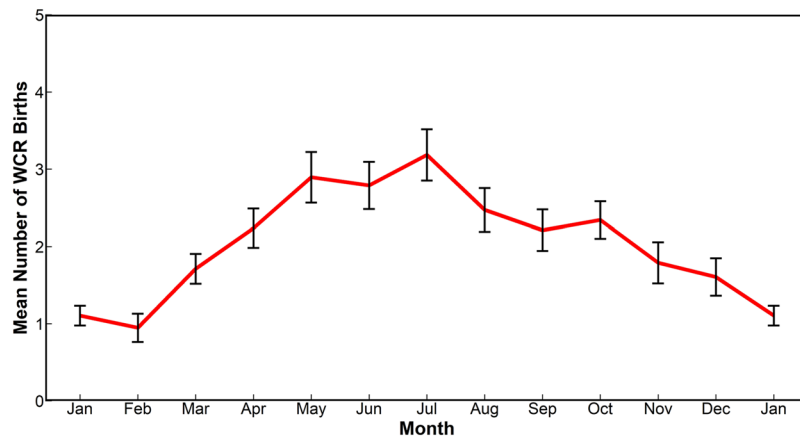


Figure 2. Seasonal Cycle of WCR formation over the whole region between 75°W and 55°W. The vertical bars denote the standard error of mean for each month.

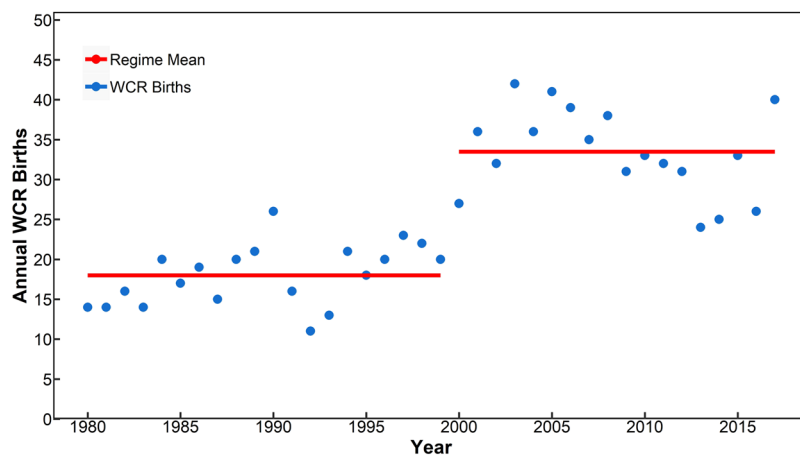


Figure 3. Interannual Variability of the WCR formation between 1980 and 2017. The regime shift (denoted by the split in the red solid line) is significant at the turn of the century.

Seasonal-to-inter-annual variability. On a seasonal scale, WCR formation peaks in late spring/early summer (May–June–July) while the wintertime (January–February) has fewer rings forming (Fig. 2). The summertime peak is also present in each of the four different sub-regions. Previous statistical studies on WCRs have also indicated that the ring production by the GS system peaks during the summer months^{23,24}.

The WCR formation process has been linked with GS instability processes, which convert the available potential energy to the eddy kinetic energy (EKE)^{33–35}. Zhai *et al.*³⁶ analyzed satellite altimeter data and found that in the GS region (73°W–44°W), EKE peaks in summer while the ocean is most baroclinically unstable during the winter. A recent numerical modeling study³⁷ found that in the GS region (75°W–55°W) EKE has a dominant peak in May and a secondary peak in September near the surface. A similar correlation between surface EKE and the baroclinic instability was observed in the North Pacific³⁸ and the southern Indian Ocean³⁹. In these cases, a theoretical model was used to show that the lag of a couple of months corresponds to the length of time for unstable waves to grow in the respective regions.

The observed annual birth of the WCRs for the whole time-period (1980–2017) is presented in Fig. 3. From a sample size of 961 WCRs, there is significant inter-annual variability in the number of WCRs formed in individual years, with a maximum occurrence of 42 in 2003 (followed by 41 in 2005 and in 2017), and a minimum occurrence of 11 WCRs in 1992. The number of WCRs in the slope sea between 75° and 55°W has significantly increased over the 38-year period (1980–2017). The inter-annual variability consists of short periods of increasing and decreasing rates of ring formation; the maximum rate was seen between 1993 and 2005, when about 2 additional rings were born every year, followed by a decreasing rate between 2005 and 2012. A more recent increasing rate (2012–2015) has been discussed briefly by Gawarkiewicz *et al.*⁴⁰ in relation to recent warming of the Gulf of Maine and Northeast Shelf ecosystem.

Regime shift around the year 2000. Given the pattern of ring formation appearing in Fig. 3, the possibility of an abrupt change in the pattern opposed to a gradual increase is worth examining. Regime shifts are a common feature of many geophysical systems^{41–44} and it is unclear a priori whether abrupt or gradual change

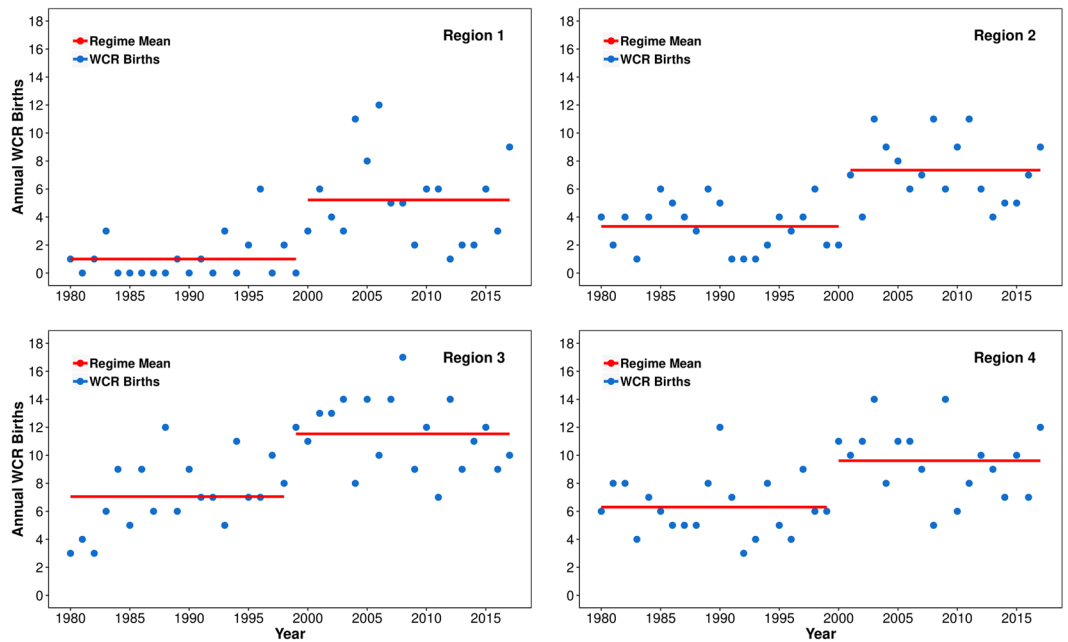


Figure 4. Interannual Variability of WCR formation in different sub-regions—Region 1: 75°–70°W; Region 2: 70°–65°W; Region 3: 65°–60°W; Region 4: 60°–55°W. Significant regime changes were detected between 1998 and 2000 for each region. See Table 1 for exact shift years.

Regime Character		Region 1 (75–70 W)	Region 2 (70–65 W)	Region 3 (65–60 W)	Region 4 (60–55 W)	Total WCR (75–55 W)
Regime #1	Period	1980–1999	1980–2000	1980–1998	1980–1999	1980–1999
	Mean	1.00	3.33	7.05	6.30	18.00
	L	20	21	19	20	20
Regime Shift	Shift	Upward	Upward	Upward	Upward	Upward
	RSI	8.47	9.24	10.84	7.34	15.25
	p-value	2.81E-05	2.17E-06	3.95E-06	1.13E-04	5.79E-11
Regime #2	Period	2000–2017	2001–2017	1999–2017	2000–2017	2000–2017
	Mean	5.22	7.35	11.53	9.61	33.39
	L	18	17	19	18	18

Table 1. Summary of statistics for the Regime Shift analysis for all regions.

should be expected in ring formation for the Gulf Stream system. In this study, a sequential-t test-based regime shift detection algorithm^{45–47} was used to identify the regimes evident in the WCR birth time-series shown in Figs 3 and 4. The method of detecting regime shift is described in the Methodology section.

It is evident that the WCR formation process has gone through a regime shift around 2000. Note that the period 1980–1999 produced a total of 360 rings (annual average of 18), while the period (2000–2017) produced a total of 601 rings (annual average of 33). Figure 4 presents the regime-shift analysis results for each of the four sub-regions. The summary statistics of the regime-shift analysis are presented in Table 1. All four sub-regions show significant regime change between 1998–2000. These results were also supported by the Change-point analysis in R⁴⁸, the Change-point detection in Matlab^{49,50} and by an independent Markov Regime Switch model⁵¹, in that these methods also detected the regime-shift for the whole area in year 2000 and for the sub-regions between 1998–2000 (see Methodology for details on these different models).

The time-series in Fig. 3 also shows an overall increasing trend that could fit a linear model. Significant p-values were obtained for both linear and regime-shift models. However, the residual variance (the variance of the residual between the observations and the model fit)⁵² was larger (36.91) for the linear model compared than for the regime-shift model (21.47). Furthermore, the regime-shift model explains 75% of the variance compared to only 56% by the linear trend. Thus we conclude that the regime-shift model renders an appropriate and robust explanation of the behavior of the WCR formation during this 38-year period.

Discussion

Three different factors are important to consider for investigating possible reasons behind such a regime shift of the WCR formation: (i) decreasing reduced gravity, (ii) internal GS dynamics and (iii) atmospheric forcing.

A typical ring formation event after the GS leaves the coast at Cape Hatteras happens when the radius of deformation is comparable to the meandering length scale^{53–55}. Dynamically, this occurs when the centrifugal force is balanced by the Coriolis force for the fluid parcels following the crest of a meander, which then becomes a closed vortex, or WCR. The internal radius of deformation (R_d) is generally given by $\left(\frac{\lambda g' H}{f}\right)$, where g' is the reduced gravity, H is the water depth, and f is the Coriolis parameter.

Therefore, a reduction of g' might lead to a smaller R_d and increased WCR formation. The observed warming in the slope waters^{4,40,56} in the past decade might have reduced the density difference between the slope water and the GS. So, the recent warming in the slope water might have contributed to the increasing number of WCRs in the later regime after 2000. Additionally, while atmospheric forcing might have led to the initial warming of the slope sea¹⁰ the latter mechanism of decreasing reduced gravity has a positive feedback by producing more WCRs giving rise to even warmer and saltier slope water.

It is also reasonable to postulate that the WCR formation is driven by the instabilities (both barotropic and baroclinic)^{53,57} generated in the GS through its interaction with the slope and Sargasso waters, with the Deep Western Boundary Current (DWBC) and with the NESC. However, the instabilities take time to grow and thus a lag between the transport of the GS at Hatteras and the WCR formation in the regions downstream might be expected as discussed in Section 2.1. In this context, the multi-year (1992–2016 and beyond) transport data for the GS, Sargasso and Slope waters available from the Oleander group^{58–60} would be very useful. A thorough instability-based analysis relating the OMV Oleander transport (of the GS, Sargasso and Slope waters), westward movement of the destabilization point of the GS⁵⁷, the DWBC strength and proximity to NESC with the number of WCRs will be forthcoming.

Further to the east, an altimetric data analysis⁶¹ showed that the GS path between 65°W and 55°W has progressively moved southward during 1993–2013. The overall increasing trend of the WCR formation over almost four decades also coincided with a recently reported southward shift east of 65°W and slowing of the GS transport^{62,63} during 1993–2016. Evidently such a southward excursion of the GS system at its eastern end would allow for more WCR birth in the 65°–55°W region and might have resulted in increased ring formation during the last seventeen years. Note that both sub-regions (65°–60°W and 60°–55°W) are the major contributors to the total ring formation numbers due to the stream's large-amplitude meandering behavior as it crosses the NESC^{32,64}. Thus, a slight additional southward displacement might enhance ring formation in this region even further due to flow interactions with the Sea Mounts.

With regards to atmospheric forcing, the North Atlantic Oscillation (NAO) has been linked to the formation of the WCRs through the GS EKE in the past^{16,35,65}. While the WCRs were inversely lag-correlated with the NAO winter Index during 1978–1999¹⁶, such a relationship with the NAO was not found during 2000–2016. It is uncertain at this time how the interannual variability of the NAO-induced winds affect the GS EKE to provide for the baroclinic instability that would be necessary to produce a large number of WCRs during the past two recent decades.

One other obvious suspect for the causes of the regime shift is the wind-stress curl over the subtropical North Atlantic that generates the westward propagating Rossby waves to generate the western boundary current^{66–69}. Recently, the decadal shifts of the Kuroshio Extension (KE) have been shown to be associated with a weak (strong) transport and unstable (stable) meandering configuration⁷⁰. These opposing phases were linked to the basin-wide wind-stress curl forced negative (positive) Sea Surface Height (SSH) anomalies propagating west in the form of Rossby waves during negative (positive) phases of the North Pacific Gyre Oscillation. Furthermore, Yang *et al.*⁷¹ recently showed that the strong and stable state of the KE is also associated with a strong southern recirculation gyre. Future studies are needed to investigate the possibility of a weakening southern recirculation gyre during the past two decades that could add to the increasingly unstable state of the GS. Such investigations should also reconcile with recent observations of westward movement of the destabilization point of the GS⁵⁷.

Such a high number of WCRs in the slope water might have impacted the ecosystem of the GOM/GB and MAB by making them even warmer and saltier in the first two decades of the twenty-first century. This is clearly evident during recent specific Ring intrusion events, for example during January 2017 south of New England when Gulf Stream flounder were caught in Rhode Island Sound in addition to juvenile Black Sea Bass⁴⁰. However, it is also likely that the increasing frequency of warm core ring encounters with the continental shelf will contribute to increased warming of the continental shelf. This in turn is likely to increase the rate at which the geographical centroid of marine species moves to the north⁷².

Conclusions

We present observational evidence that the number of WCRs formed from the GS has undergone a significant regime-shift at around the year 2000. The average number of WCR formations has increased to 33 per year during 2000–2017 from an average of 18 per year during 1980–1999. We hypothesize that the increase of the number of WCRs in recent years could be related to increased instability due to several factors, such as (i) decreasing reduced gravity between the slope and the GS due to warming of the slope (via atmospheric forcing), (ii) internal dynamics of the GS system (including transport, latitudinal movement, and interactions with DWBC and NESC), and (iii) changes in the large-scale atmospheric forcing, or a combination of these factors. Further detailed simulations and energetics analysis will be necessary to quantify these relationships and identify the dynamics behind the increased number of WCRs since 2000.

Methodology

Data. The primary dataset is a set of charts prepared by one of the co-authors, Jenifer Clark (JC). An example is shown in Fig. 1a. This collection of charts of the GS and surrounding waters has been annotated with satellite data indicating temperature. Using infra-red (IR) imagery, satellite altimetry data, and surface *in-situ* temperature data, oceanographic analyses were produced for this region in the form of 2–3 day composite charts in a

consistent manner. These charts show the location, extent and temperature signature of currents (GS, shelf-slope front), warm and cold-core rings (WCRs and CCRs), other eddies, shingles, intrusions and other water mass boundaries in the Gulf of Maine, over Georges Bank and in the Middle Atlantic Bight.

These charts have been used in the past by various researchers for different purposes. Some studies^{23,24,29} have used these over different 5-year periods in the 1980s to develop a WCR climatology and related statistics. These charts were used for the first synoptic prediction of cold-core-ring propagation and their acoustic signatures for the US Navy⁵³. Such charts were also used for interannual variability studies¹⁶ and for IOOS-related operational forecasting^{73,74}.

The basis data source was individual IR temperature images from the NOAA polar orbiting satellites (NOAA-5 in the early 1980s to NOAA-18 recently) at 6–12 hourly intervals. These images were captured by the Advanced Very High Resolution Radiometer (AVHRR) and AVHRR2 instruments, both of which had a resolution of 1.1 km over the last four decades. Each individual image has a different lookup table (or colormap) for temperature that resolves 256 distinct sets of intensity, hue and saturation of color within the available and retrievable IR signal range. This allows for accurate identification of the small-scale features in each image. The analyst locates all of the small scale features in each individual satellite SST image within a three-day period. The locations and boundaries of the features (GS, WCR, CCR and other smaller scale entities) are remapped onto a 3-day composite image for that period. The 3-day composite image has a fixed and broad (5–30 °C) range of temperature with similar 256-set indexing, which by itself could not resolve the features. Note that individual images with high-resolution within a narrower band of temperature range also have clouds, which are eliminated (or at least minimized) during the process of generating the 3-day composites. The 3-day composite helps to visualize the whole GS and its rings in a broader region (like Fig. 1a); while the individual images help resolve the features at a very high resolution. The 3-day composite images are regularly produced by NOAA and/or the Johns Hopkins University Applied Physics Lab (fermi) group (see <http://fermi.jhuapl.edu> for more details). Thus, the JC Charts, which uses this basis data source, is the most continuous and consistent data set to extract the WCRs, the GS and the CCRs over the whole period of analysis (1980–2017) at a constant resolution of 1.1 km^{30,31}.

The process of creating the WCR census time-series can be summarized as follows. First, the JC Charts are available 2–3 times a week from 1980–2017. Thus, we used approximately 5000 Charts for the 38 years of analysis. All of these charts were reanalyzed between 75° and 55°W using QGIS 2.18.16⁷⁵ and georeferenced on a WGS84 coordinate system⁷⁶. The analyst goes through each chart and follows a set of rules (birth, continuity, death) to identify each WCR³⁰ and tabulates the ring parameters. A new ring formation is documented in the following situations: (i) a typical GS crest forming a closed anticyclonic vortex and detaches from the stream in the slope water; (ii) an anticyclonic eddy forms off of another large anticyclonic eddy in the slope water; (iii) an anticyclonic eddy further away from the stream coming into the domain through Region 4³⁰. Note that any anticyclonic eddy that existed for less than 7 days was not counted in the census.

Thirty-eight years of WCR census yielded a total of 961 WCRs and their birth, death, size and age information were documented and are available on request. In addition, we also have access to a database from Roger Pettipas of BIO who documented the ring center location, and size at birth on each analysis day, generally twice a week from the same set of JC Charts (also called the NOAA Charts) during the period 1980–2004. A validation was carried out^{30,31} using the BIO data, an earlier study¹⁶ and this new Census to eliminate the possibility of any analyst error. A similar and comprehensive Census development for the CCRs of the GS system using the GIS framework is underway.

Regime shift analysis. A sequential regime shift detection algorithm^{45–47} was used to identify the regimes evident in the WCR birth time-series shown in Fig. 1 for the whole and all four sub-regions. The algorithm detects the regime shifts in the mean and the variance. Briefly, the method includes applying the student's T-Test sequentially to a time-series when data is arriving continuously. With the arrival of a new observation to its time-series, a check is performed to determine whether the deviation of the current mean, \bar{x}_{cur} , from the new mean, \bar{x}_{new} (including the new observation), is statistically significant or not. A key factor is the choice of the cut-off length to start the sequencing that was varied between 5 and 21 years for this 38-year period of study. The regimes presented in Table 1 are found to be stable at 95% confidence interval in the range of variation of cut-off length 5–21. In the second step, when \bar{x}_{new} is significantly different from \bar{x}_{cur} , a second criterion, based on a quantity called the 'Regime Shift Index' (RSI) is invoked. RSI represents the cumulative sum of normalized anomalies over the current period of analysis (see Rodionov⁴⁵ for the exact equation and its explanation). A regime shift is detected when the new regime mean shows an upward (downward) shift and RSI is negative (positive) and t_{cur} is declared as the change point by the algorithm⁴⁶.

The Changepoint analysis in R⁴⁸ tests for sequential changes in the mean by testing for the null hypothesis (H_0) that corresponds to no change point using a likelihood based framework. The test statistic is constructed using the Maximum Log Likelihood value for the change point. If this Maximum Log Likelihood value is higher than a threshold value then the test rejects the hypothesis.

The Changepoint detection in Matlab^{49,50} involves choosing a point in a timeseries dividing the series into two sections. The total residual error for each section is calculated using the difference between series points and the empirical mean (and/or variance). The change point is decided when the total residual error is at a minimum.

The Markov Regime Shift Models⁵¹ allows for detecting multiple states in a time-series based on estimation of Maximum Log Likelihood⁷⁷. Since the states are unknown, this method involves estimating the Maximum Log Likelihood as a weighted average of the state's probability distributions. The probabilities of each state are determined by filtered probabilities^{78,79} that use available information of each state based on arrival of new information. A 2-state model was used in this study to detect the regime-shift of the WCR formation.

Data Availability

The datasets generated during and/or analyzed during the current study are available from the corresponding author on reasonable request.

References

- Andres, M., Gawarkiewicz, G. G. & Toole, J. M. Interannual sea level variability in the western North Atlantic: Regional forcing and remote response. *Geophys. Res. Lett.* **40**, 5915–5919, <https://doi.org/10.1002/2013GL058013> (2013).
- Mills, K. E. *et al.* Fisheries management in a changing climate: lessons from the 2012 ocean heat wave in the Northwest. *Atlantic Oceanography* **26**, 191–195, <https://doi.org/10.5670/oceanog.2013.27> (2013).
- Han, G., Chen, N. & Ma, Z. Is there a north-south phase shift in the surface Labrador Current transport on the interannual-to-decadal scale? *Journal of Geophysical Research: Oceans* **119**, 276–287, <https://doi.org/10.1002/2013JC009102> (2014).
- Forsyth, J. S. T., Andres, M. & Gawarkiewicz, G. G. Recent accelerated warming of the continental shelf off New Jersey: Observations from the CMV Oleander expendable bathythermograph line. *Journal of Geophysical Research: Oceans* **120**, 2370–2384, <https://doi.org/10.1002/2014JC010516> (2015).
- Pershing, A. J. *et al.* Slow adaptation in the face of rapid warming leads to collapse of the Gulf of Maine cod fishery. *Science* **350**, 809–812, <https://doi.org/10.1126/science.aac9819> (2015).
- Robson, J., Ortega, P. & Sutton, R. A reversal of climatic trends in the North Atlantic since 2005. *Nature Geoscience* **9**, 513, <https://doi.org/10.1038/ngeo2727> (2016).
- Perretti, C. T. *et al.* Regime shifts in fish recruitment on the Northeast US Continental Shelf. *Mar. Ecol. Prog. Ser.* **574**, 1–11, <https://doi.org/10.3354/meps12183> (2017).
- Palmer, M. Assessment update report of the Gulf of Maine Atlantic cod stock. *US Dept Commer, Northeast Fish Sci Cent Ref Doc* **119**, <https://doi.org/10.7289/V5V9862C> (2014).
- Nye, J. A., Link, J. S., Hare, J. A. & Overholtz, W. J. Changing spatial distribution of fish stocks in relation to climate and population size on the Northeast United States continental shelf. *Mar. Ecol. Prog. Ser.* **393**, 111–129, <https://doi.org/10.3354/meps08220> (2009).
- Chen, K., Gawarkiewicz, G., Kwon, Y. & Zhang, W. G. The role of atmospheric forcing versus ocean advection during the extreme warming of the Northeast US continental shelf in 2012. *Journal of Geophysical Research: Oceans* **120**, 4324–4339, <https://doi.org/10.1002/2014JC010547> (2015).
- Chen, K., Gawarkiewicz, G. G., Lentz, S. J. & Bane, J. M. Diagnosing the warming of the Northeastern US Coastal Ocean in 2012: A linkage between the atmospheric jet stream variability and ocean response. *Journal of Geophysical Research: Oceans* **119**, 218–227, <https://doi.org/10.1002/2013JC009393> (2014).
- Bisagni, J. Lagrangian current measurements within the eastern margin of a warm-core Gulf Stream ring. *J. Phys. Oceanogr.* **13**, 709–715, 10.1175/1520-0485(1983)013<0709:LCMWTE>2.0.CO;2 (1983).
- Ramp, S., Beardsley, R. & Legeckis, R. An observation of frontal wave development on a shelf-slope/warm core ring front near the shelf break south of New England. *J. Phys. Oceanogr.* **13**, 907–912, 10.1175/1520-0485(1983)013<0907:AOFWD>2.0.CO;2 (1983).
- Joyce, T. M. & McDougall, T. J. Physical structure and temporal evolution of Gulf Stream warm-core ring 82B. *Deep Sea Research Part A. Oceanographic Research Papers* **39**, S19–S44, [https://doi.org/10.1016/S0198-0149\(11\)80003-8](https://doi.org/10.1016/S0198-0149(11)80003-8) (1992).
- Gawarkiewicz, G., Bahr, F., Beardsley, R. C. & Brink, K. H. Interaction of a slope eddy with the shelfbreak front in the Middle Atlantic Bight. *J. Phys. Oceanogr.* **31**, 2783–2796, 10.1175/1520-0485(2001)031<2783:IOASEW>2.0.CO;2 (2001).
- Chaudhuri, A. H., Gangopadhyay, A. & Bisagni, J. J. Interannual variability of Gulf Stream warm core rings in response to the North Atlantic Oscillation. *Cont. Shelf Res.* **29**, 856–869, <https://doi.org/10.1016/j.csr.2009.01.008> (2009).
- Zhang, W. G. & Gawarkiewicz, G. G. Dynamics of the direct intrusion of Gulf Stream ring water onto the Mid-Atlantic Bight shelf. *Geophys. Res. Lett.* **42**, 7687–7695, <https://doi.org/10.1002/2015GL065530> (2015).
- Saunders, P. M. Anticyclonic eddies formed from shoreward meanders of the Gulf Stream. *Deep Sea Research and Oceanographic Abstracts Ser.* **18**, 1207–1219, [https://doi.org/10.1016/0011-7471\(71\)90027-1](https://doi.org/10.1016/0011-7471(71)90027-1) (1971).
- Lai, D. Y. & Richardson, P. L. Distribution and movement of Gulf Stream rings. *J. Phys. Oceanogr.* **7**, 670–683, 10.1175/1520-0485(1977)007<0670:DAMOGS>2.0.CO;2 (1977).
- Joyce, T. M. Gulf Stream warm-core ring collection: An introduction. *Journal of Geophysical Research: Oceans* **90**, 8801–8802, <https://doi.org/10.1029/JC090iC05p08801> (1985).
- Bisagni, J. J. In *Passage of anticyclonic Gulf Stream eddies through Deepwater Dumpsite 106 during 1974 and 1975*. (US Dept of Commerce Pub, 1976).
- Halliwel, G. R. & Mooers, C. N. The space-time structure and variability of the shelf water-slope water and Gulf Stream surface temperature fronts and associated warm-core eddies. *Journal of Geophysical Research: Oceans* **84**, 7707–7725, <https://doi.org/10.1029/JC084iC12p07707> (1979).
- Brown, O. B., Cornillon, P. C., Emmerson, S. R. & Carle, H. M. Gulf Stream warm rings: A statistical study of their behavior. *Deep Sea Research Part A. Oceanographic Research Papers* **33**, 1459–1473, [https://doi.org/10.1016/0198-0149\(86\)90062-2](https://doi.org/10.1016/0198-0149(86)90062-2) (1986).
- Auer, S. J. Five-year climatological survey of the Gulf Stream system and its associated rings. *Journal of Geophysical Research: Oceans* **92**, 11709–11726, <https://doi.org/10.1029/JC092iC11p11709> (1987).
- Flierl, G. R. The application of linear quasigeostrophic dynamics to Gulf Stream rings. *J. Phys. Oceanogr.* **7**, 365–379, 10.1175/1520-0485(1977)007<0365:TAOLQD>2.0.CO;2 (1977).
- Csanady, G. The birth and death of a warm core ring. *Journal of Geophysical Research: Oceans* **84**, 777–780, <https://doi.org/10.1029/JC084iC02p00777> (1979).
- Olson, D., Schmitt, R., Kennelly, M. & Joyce, T. A two-layer diagnostic model of the long-term physical evolution of warm core ring 82B. *Journal of Geophysical Research: Oceans* **90**, 8813–8822, <https://doi.org/10.1029/JC090iC05p08813> (1985).
- Chen, K. & He, R. Mean circulation in the coastal ocean off northeastern North America from a regional-scale ocean model. *Ocean Science* **11**, 503–517, <https://doi.org/10.5194/os-11-503-2015> (2015).
- Cerone, J. F. Satellite observed climatology of warm core Gulf Stream rings and discussion of their possible biological effects (1984).
- Monim, M. Seasonal and Inter-annual Variability of Gulf Stream Warm Core Rings from 2000 to 2016. MS Thesis, University of Massachusetts Dartmouth, 113 pp (2017).
- Silva, E. Understanding Thirty-Eight years of Gulf Stream's Warm Core Rings: Variability, Regimes and Survival. MS Thesis, University of Massachusetts Dartmouth, 125 pp (2019).
- Cornillon, P. The effect of the New England Seamounts on Gulf Stream meandering as observed from satellite IR imagery. *J. Phys. Oceanogr.* **16**, 386–389, 10.1175/1520-0485(1986)016<0386:TEOTNE>2.0.CO;2 (1986).
- Gill, A., Green, J. & Simmons, A. Energy partition in the large-scale ocean circulation and the production of mid-ocean eddies. *Deep-Sea Res.* **21**, 499–528, [https://doi.org/10.1016/0011-7471\(74\)90010-2](https://doi.org/10.1016/0011-7471(74)90010-2) (1974).
- Robinson, A. R. *et al.* Forecasting Gulf Stream meanders and rings. *Eos, Transactions American Geophysical Union* **70**, 1464–1473, <https://doi.org/10.1029/89EO00346> (1989).
- Stammer, D. & Wunsch, C. Temporal changes in eddy energy of the oceans. *Deep Sea Research Part II: Topical Studies in Oceanography* **46**, 77–108, [https://doi.org/10.1016/S0967-0645\(98\)00106-4](https://doi.org/10.1016/S0967-0645(98)00106-4) (1999).

36. Zhai, X., Greatbatch, R. J. & Kohlmann, J. On the seasonal variability of eddy kinetic energy in the Gulf Stream region. *Geophys. Res. Lett.* **35**, <https://doi.org/10.1029/2008GL036412> (2008).
37. Kang, D., Curchitser, E. N. & Rosati, A. Seasonal variability of the Gulf Stream kinetic energy. *J. Phys. Oceanogr.* **46**, 1189–1207, <https://doi.org/10.1175/JPO-D-15-0235.1> (2016).
38. Qiu, B. Seasonal eddy field modulation of the North Pacific Subtropical Countercurrent: TOPEX/Poseidon observations and theory. *J. Phys. Oceanogr.* **29**, 2471–2486, [10.1175/1520-0485\(1999\)029<2471:SEFMOT>2.0.CO;2](https://doi.org/10.1175/1520-0485(1999)029<2471:SEFMOT>2.0.CO;2) (1999).
39. Jia, F., Wu, L. & Qiu, B. Seasonal modulation of eddy kinetic energy and its formation mechanism in the southeast Indian Ocean. *J. Phys. Oceanogr.* **41**, 657–665, <https://doi.org/10.1175/2010JPO4436.1> (2011).
40. Gawarkiewicz, G. *et al.* The changing nature of shelf-break exchange revealed by the OOI Pioneer Array. *Oceanography* **31**, 60–70, <https://doi.org/10.5670/oceanog.2018.110> (2018).
41. Kerr, R. A. Unmasking a shifty climate system. *Science* **255**, 1508, <https://doi.org/10.1126/science.255.5051.1508> (1992).
42. Mantua, N. J., Hare, S. R., Zhang, Y., Wallace, J. M. & Francis, R. C. A Pacific interdecadal climate oscillation with impacts on salmon production. *Bull. Am. Meteorol. Soc.* **78**, 1069–1080, [10.1175/1520-0477\(1997\)078<1069:APICOW>2.0.CO;2](https://doi.org/10.1175/1520-0477(1997)078<1069:APICOW>2.0.CO;2) (1997).
43. Hare, S. R. & Mantua, N. J. Empirical evidence for North Pacific regime shifts in 1977 and 1989. *Prog. Ocean.* **47**, 103–145, [https://doi.org/10.1016/S0079-6611\(00\)00033-1](https://doi.org/10.1016/S0079-6611(00)00033-1) (2000).
44. Reid, P. C. *et al.* Global impacts of the 1980s regime shift. *Global Change Biol.* **22**, 682–703, <https://doi.org/10.1111/gcb.13106> (2016).
45. Rodionov, S. N. A sequential algorithm for testing climate regime shifts. *Geophys. Res. Lett.* **31**, <https://doi.org/10.1029/2004GL019448> (2004).
46. Rodionov, S. & Overland, J. E. Application of a sequential regime shift detection method to the Bering Sea ecosystem. *ICES J. Mar. Sci.* **62**, 328–332, <https://doi.org/10.1016/j.icesjms.2005.01.013> (2005).
47. Rodionov, S. N. Use of prewhitening in climate regime shift detection. *Geophys. Res. Lett.* **33**, <https://doi.org/10.1029/2006GL025904> (2006).
48. Killick, R., Eckley, I. & Haynes, K. Changepoint: An R package for changepoint analysis, 2013. *R package version*, **1**(5) (2015).
49. Mathworks. MATLAB - Changepoint Detection (2016).
50. Killick, R., Fearnhead, P. & Eckley, I. A. Optimal detection of changepoints with a linear computational cost. *Journal of the American Statistical Association* **107**(500), 1590–1598 (2012).
51. Perlin, M. MS_Regress—The MATLAB package for Markov regime switching models. 2012. Available at SSRN (2014).
52. Weisberg, S. In *Applied linear regression* (John Wiley & Sons, 2005).
53. Robinson, A. R., Spall, M. A. & Pinardi, N. Gulf Stream simulations and the dynamics of ring and meander processes. *J. Phys. Oceanogr.* **18**, 1811–1854, [10.1175/1520-0485\(1988\)018<1811:GSSATD>2.0.CO;2](https://doi.org/10.1175/1520-0485(1988)018<1811:GSSATD>2.0.CO;2) (1988).
54. Chassignet, E. P. & Cushman-Roisin, B. On the influence of a lower layer on the propagation of nonlinear oceanic eddies. *J. Phys. Oceanogr.* **21**, 939–957, [10.1175/1520-0485\(1991\)021<0939:OTIOAL>2.0.CO;2](https://doi.org/10.1175/1520-0485(1991)021<0939:OTIOAL>2.0.CO;2) (1991).
55. Olson, D. B. Rings in the ocean. *Annu. Rev. Earth Planet. Sci.* **19**, 283–311, <https://doi.org/10.1146/annurev.ea.19.050191.001435> (1991).
56. Chen, K., Kwon, Y. & Gawarkiewicz, G. Interannual variability of winter-spring temperature in the Middle Atlantic Bight: Relative contributions of atmospheric and oceanic processes. *Journal of Geophysical Research: Oceans* **121**, 4209–4227, <https://doi.org/10.1002/2016JC011646> (2016).
57. Andres, M. On the recent destabilization of the Gulf Stream path downstream of Cape Hatteras. *Geo. Res. Lett.* **43**, 9836–9842, <https://doi.org/10.1002/2016GL069966> (2016).
58. Rossby, T., Flagg, C. & Donohue, K. On the variability of Gulf Stream transport from seasonal to decadal timescales. *J. Mar. Res.* **68**, 503–522, <https://doi.org/10.1357/002224010794657128> (2010).
59. Rossby, T., Flagg, C., Donohue, K., Sanchez-Franks, A. & Lillibridge, J. On the long-term stability of Gulf Stream transport based on 20 years of direct measurements. *Geophys. Res. Lett.* **41**, 114–120, <https://doi.org/10.1002/2013GL058636> (2014).
60. Sanchez-Franks, A., Flagg, C. & Rossby, T. A comparison of transport and position between the Gulf Stream east of Cape Hatteras and the Florida Current. *J. Mar. Res.* **72**, 291–306, <https://doi.org/10.1357/002224014815460641> (2014).
61. Bisagni, J. J., Gangopadhyay, A. & Sanchez-Franks, A. Secular change and Interannual variability of the Gulf Stream position, 1993–2013, 70°–55° W. *Deep Sea Research Part I: Oceanographic Research Papers* **125**, 1–10, <https://doi.org/10.1016/j.dsr.2017.04.001> (2017).
62. Ezer, T., Atkinson, L. P., Corlett, W. B. & Blanco, J. L. Gulf Stream's induced sea level rise and variability along the US mid-Atlantic coast. *Journal of Geophysical Research: Oceans* **118**, 685–697, <https://doi.org/10.1002/jgrc.20091> (2013).
63. Dong, S., Baringer, M. O. & Goni, G. J. Slow Down of the Gulf Stream during 1993–2016, *Nature – Scientific Reports*, 9(1), <https://doi.org/10.1038/s41598-019-42820-8> (2019).
64. Lee, T. & Cornillon, P. Propagation and growth of Gulf Stream meanders between 75 and 45 W. *J. Phys. Oceanogr.* **26**, 225–241, [10.1175/1520-0485\(1996\)026<0225:PAGOGS>2.0.CO;2](https://doi.org/10.1175/1520-0485(1996)026<0225:PAGOGS>2.0.CO;2) (1996).
65. Penduff, T., Barnier, B., Dewar, W. K. & O'Brien, J. J. Dynamical response of the oceanic eddy field to the North Atlantic Oscillation: A model–data comparison. *Journal of Physical Oceanography*, **34**(12), 2615–2629 (2004).
66. Gill, A. E. In *International Geophysics, 30: Atmosphere-ocean Dynamics* (Elsevier, 1982).
67. Gangopadhyay, A., Cornillon, P. & Watts, D. R. A test of the Parsons–Veronis hypothesis on the separation of the Gulf Stream. *J. Phys. Oceanogr.* **22**, 1286–1301, [10.1175/1520-0485\(1992\)022<1286:ATOTPH>2.0.CO;2](https://doi.org/10.1175/1520-0485(1992)022<1286:ATOTPH>2.0.CO;2) (1992).
68. Dengg, J., Beckmann, A. & Gerdes, R. In *The warmwatersphere of the North Atlantic Ocean* (Krauss, W. ed.) 253–290, (Gebrüder Borntraeger, 1996).
69. Haidvogel, D. B. & Beckmann, A. In *Numerical ocean circulation modeling* (Imperial College Press, 1999).
70. Qiu, B. & Chen, S. Eddy-mean flow interaction in the decadal modulating Kuroshio Extension system. *Deep Sea Research Part II: Topical Studies in Oceanography* **57**, 1098–1110, <https://doi.org/10.1016/j.dsr2.2008.11.036> (2010).
71. Yang, Y. & San Liang, X. On the Seasonal Eddy Variability in the Kuroshio Extension. *J. Phys. Oceanogr.* **48**, 1675–1689, <https://doi.org/10.1175/JPO-D-18-0058.1> (2018).
72. Pinsky, M. L., Worm, B., Fogarty, M. J., Sarmiento, J. L. & Levin, S. A. Marine taxa track local climate velocities. *Science* **341**, 1239–1242, <https://doi.org/10.1126/science.1239352> (2013).
73. Schofield, O. *et al.* Automated sensor network to advance ocean science. *Eos, Transactions American Geophysical Union* **91**, 345–346, <https://doi.org/10.1029/2010EO390001> (2010).
74. Gangopadhyay, A., Schmidt, A., Agel, L., Schofield, O. & Clark, J. Multiscale forecasting in the western North Atlantic: Sensitivity of model forecast skill to glider data assimilation. *Cont. Shelf Res.* **63**, S159–S176, <https://doi.org/10.1016/j.csr.2012.09.013> (2013).
75. QGIS Development Team. QGIS Geographic Information System (2016).
76. Decker, B. L. World Geodetic System 1984. *World geodetic system 1984* (1986).
77. Hamilton, J. & Raj, B. In *Advances in Markov-Switching Models*. (Springer, 2005).
78. Hamilton, J. D. & Susmel, R. Autoregressive conditional heteroskedasticity and changes in regime. *J. Econ.* **64**, 307–333, [https://doi.org/10.1016/0304-4076\(94\)90067-1](https://doi.org/10.1016/0304-4076(94)90067-1) (1994).
79. Kim, C. & Nelson, C. R. In *State-space models with regime switching* (MIT Press 1999).

Acknowledgements

The authors acknowledge financial supports from NOAA (NA11NOS0120038), NSF (OCE-0815679), SMAST and UMass Dartmouth. GG was supported by NSF under grant OCE-1657853 as well as a Senior Scientist Chair from WHOI. We have benefitted from many discussions on GS system behavior and variability with Tom Rossby, Charlie Flagg, Kathy Donohue, Randy Watts, Peter Cornillon, Magdalena Andres and on WCR identification with Jim Bisagni. The WCR data from Jenifer Clark (co-author) and Roger Pettipas were used to develop the original census. We wish to thank the Editor and two anonymous reviewers for their helpful comments and encouragement to a previous version which improved the focus of this manuscript.

Author Contributions

A.G. and G.G. conceived the overall questions and analyzed the data. J.C. provided the archive of charts from 1980 to 2017. N.S. and M.M. created the WCR census. N.S. created the figures and performed the Regime Shift Analysis. A.G. and G.G. wrote the final version with inputs from N.S., M.M. and J.C.

Additional Information

Competing Interests: The authors declare no competing interests.

Publisher's note: Springer Nature remains neutral with regard to jurisdictional claims in published maps and institutional affiliations.



Open Access This article is licensed under a Creative Commons Attribution 4.0 International License, which permits use, sharing, adaptation, distribution and reproduction in any medium or format, as long as you give appropriate credit to the original author(s) and the source, provide a link to the Creative Commons license, and indicate if changes were made. The images or other third party material in this article are included in the article's Creative Commons license, unless indicated otherwise in a credit line to the material. If material is not included in the article's Creative Commons license and your intended use is not permitted by statutory regulation or exceeds the permitted use, you will need to obtain permission directly from the copyright holder. To view a copy of this license, visit <http://creativecommons.org/licenses/by/4.0/>.

© The Author(s) 2019